Biochemical and Biophysical Research Communications 443 (2014) 495–499

Contents lists available at ScienceDirect

Biochemical and Biophysical Research Communications

journal homepage: www.elsevier.com/locate/ybbrc

The N-terminal strand modulates immunoglobulin light chain fibrillogenesis

Luis del Pozo-Yauner [a,*], Jonathan S. Wall [b], Martín González Andrade [a], Rosana Sánchez-López [c], Sandra L. Rodríguez-Ambriz [d], Julio I. Pérez Carreón [a], Adrián Ochoa-Leyva [f], D. Alejandro Fernández-Velasco [e]

[a] Instituto Nacional de Medicina Genómica, Periférico Sur No. 4809, Col. Arenal Tepepan, Delegación Tlalpan, México, D.F. C.P. 14610, Mexico
[b] Departments of Radiology and Medicine, The University of Tennessee Medical Center, 1924 Alcoa Highway, Knoxville, TN, USA
[c] Instituto de Biotecnología, Universidad Nacional Autónoma de México, Av. Universidad #2001, Col. Chamilpa Cuernavaca, Morelos C.P. 62210, Mexico
[d] Centro de Desarrollo de Productos Bióticos, Instituto Politécnico Nacional, Calle CEPROBI No. 8, Col. San Isidro, Yautepec, Morelos C.P. 62731, Mexico
[e] Laboratorio de Fisicoquímica e Ingeniería de Proteínas, Departamento de Bioquímica, Facultad de Medicina, Universidad Nacional Autónoma de México, Circuito Interior, Ciudad Universitaria, Av. Universidad 3000, México, D.F. C.P. 04510, Mexico
[f] Unidad de Genómica de Poblaciones Aplicada a la Salud, Facultad de Química, UNAM-Instituto Nacional de Medicina Genómica (INMEGEN), Periférico Sur No. 4809, Col. Arenal Tepepan, Delegación Tlalpan México, D.F. C.P. 14610, Mexico

ARTICLE INFO

Article history:
Received 20 November 2013
Available online 7 December 2013

Keywords:
Light chain
Amyloid
Misfolding
Aggregation
Folding thermodynamics

ABSTRACT

It has been suggested that the N-terminal strand of the light chain variable domain (V_L) protects the molecule from aggregation by hindering spurious intermolecular contacts. We evaluated the impact of mutations in the N-terminal strand on the thermodynamic stability and kinetic of fibrillogenesis of the V_L protein 6aJL2. Mutations in this strand destabilized the protein in a position-dependent manner, accelerating the fibrillogenesis by shortening the lag time; an effect that correlated with the extent of destabilization. In contrast, the effect on the kinetics of fibril elongation, as assessed in seeding experiments was of different nature, as it was not directly dependant on the degree of destabilization. This finding suggests different factors drive the nucleation-dependent and elongation phases of light chain fibrillogenesis. Finally, taking advantage of the dependence of the Trp fluorescence upon environment, four single Trp substitutions were made in the N-terminal strand, and changes in solvent exposure during aggregation were evaluated by acrylamide-quenching. The results suggest that the N-terminal strand is buried in the fibrillar state of 6aJL2 protein. This finding suggest a possible explanation for the modulating effect exerted by the mutations in this strand on the aggregation behavior of 6aJL2 protein.

1. Introduction

Evidence suggests that the self-assembly of immunoglobulin light chains into amyloid fibrils is a misfolding phenomenon, that is promoted by factors destabilizing the native domain structure [1]. Little is known about the mechanism of AL fibril assembly or which region of the light chain forms the β-sheet core of the fibrillar aggregates. Studies conducted on the λ6 recombinant (*r*) variable domain (V_L) protein 6aJL2 suggested that the N-terminal strand (residues 1–14) is involved in the mechanism of the AL fibril assembly. It was shown that substitution of Arg25 for Gly, which disrupts the cation-π interaction between Phe2 and Arg25, increases the propensity of the protein to aggregate as amyloid fibrils *in vitro* [2]. As the Phe2–Arg25 interaction stabilizes the conformation of the N-terminus in 6aJL2 [3] (Fig. S1A and B), it was suggested that some type of structural rearrangement involving the N-terminal strand is required for the fibrillar aggregation to occur [2]. Further evidence for this hypothesis was obtained when we studied the structural role of Pro7, the residue stabilizing the sheet-switch motif that characterizes the native conformation of N-terminal strand (Fig. S1A). It was shown that the Pro7Ser substitution destabilizes the protein by 2.1 kcal/mol, and favors fibril formation. The P7S mutant showed a rearrangement of the sheet-switch motif that was accompanied by intermolecular β–β interactions involving the N-terminus and β-strand B of symmetry-related molecules in the crystal lattice [4]. Such interactions appear to be a reminiscent of the β–β contacts postulated for the cross-β structure in the amyloid fibril. Taken together, these findings reinforce the protective role hypothesis of the N-terminal strand [5], so that its destabilization and subsequent rearrangement is required for the self-assembly of the light chain into fibrils. Here, we further evaluated the structural role of the N-terminal strand in λ6 light chains by studying the effect of mutations of

* Corresponding author. Fax: +52 55 5350 1999.
E-mail address: ldelpozo@inmegen.gob.mx (L. del Pozo-Yauner).

0006-291X/$ - see front matter © 2013 Elsevier Inc. All rights reserved.
http://dx.doi.org/10.1016/j.bbrc.2013.11.123

Phe2, the hydrophobic member of the Phe2–Arg25, cation-π interaction; and Pro7 and His8, located in the sheet-switch motif. We found that mutations in these three positions significantly modulated the aggregation behavior of 6aJL2 protein. Finally, we generated single Trp substitutions at four different positions of the N-terminal strand, and evaluated, by acrylamide-quenching, the changes in their solvent exposure during aggregation. These data suggest that the N-terminal strand is buried in the fibrillar state of 6aJL2 protein.

2. Materials and methods

2.1. Site-directed mutagenesis

The cloning of the wild-type protein 6aJL2 and the mutants 6aJL2-P7S, -H8S, -H8P and -P7S-H8S were described previously [2,4]. Mutants 6aJL2-F2A, -F2S, -F2P, -F2L, -F2W, -N1W, -M3W, -H8W, and -S14W were generated by polymerase chain reaction (PCR) using pSyn1-6aJL2 construct as template in a two-step strategy, as described elsewhere [4]. The complete sequence of all the synthetic oligonucleotides used in this study are available upon request.

2.2. Bacterial expression, and purification of the rV_L λ6 proteins

The bacterial expression and purification of the rV_L proteins was performed as described previously [2].

2.3. GndHCl and thermal induced-equilibrium unfolding

Equilibrium unfolding experiments of the mutants 6aJL2-F2A, -F2S, -F2P, -F2L, -F2W were performed by addition of guanidine hydrochloride (GndHCl) and by heating, as was previously described [6].

2.4. In vitro fibrillogenesis

The *in vitro* fibrillogenesis of the λ6 proteins from the soluble precursor was performed in a 100 μg/mL (8.3 μM) protein dilution in PBS, pH 7.4, containing 20 μM of Thioflavin T (ThT) and 0.05% sodium azide, according to the method described previously [4]. The value of the lag time (t_{lag}) was calculated by extrapolation of the linear region of the hyperbolic phase to abscissa [7].

2.5. Seeding assays

Seeding experiments were performed according to the method describe previously [6]. The set of proteins tested included the wild-type 6aJL2, seven single mutants at positions 2, 7 or 8, (6a-F2S, 6a-F2L, 6a-F2P, 6a-F2W, 6a-P7S, 6a-H8S and 6a-H8P) and the double mutant 6a-P7S-H8S. The experimental sample consisted of a mixture containing 218 μg/mL (18 μM) of soluble monomer in PBS, 21.6 μg/mL of seeds (1.8 μM) and 33 μM ThT. Fluorescence data were measured using excitation and emission wavelength of 450 and 485 nm, respectively. Each sample was tested in quadruplicate. Fluorescence data were analyzed by non-linear fitting with the equation:

$$F_{ThT} = A_{ThT}(1 - e^{-kx}) \quad (1)$$

where F_{ThT} is the ThT fluorescence, A_{ThT} is the asymptotic ThT fluorescence value, and $k(s^{-1})$ is the growth rate constant of the polymerization reaction. A pseudo-first order rate constant (ks^{-1}) of the polymerization reaction was calculated by linear fitting of the data $\ln[A_{ThT} - F_t]$ as a function of time (s), where F_t is the ThT fluorescence as a function of time [8]. A_{ThT}, an indirect measure of the apparent mass of fibrils accumulated after completion of the elongation, was normalized to the wild-type 6aJL2, in order to facilitate the comparisons among proteins.

2.6. Acrylamide quenching

Samples (800 μl) 0.5 mg/mL of mutants 6aJL2-N1W, -M3W, -H8W and -S12W, diluted in PBS pH 7.4, were placed in 2.0 ml volume, capped polypropylene microtubes and incubated at 37 °C with constant agitation (1000 rpm) in a Thermomixer Confort apparatus (Eppendorf, Barkhausenweg 1, 22339 Hamburg, Germany). At predetermined times an aliquot (25 μl) was withdrawn from each sample and mixed with 2.0 ml PBS pH 7.4. Intrinsic fluorescence spectra were registered without quencher and upon adding a series of 15 μL aliquots of a 3.0 M acrylamide solution. Fluorescence measurements were performed at 25 °C in a Horiba Yvon-Jobin FluoroLog-3 spectrofluorometer (Horiba Scientific, 3880 Park Avenue, Edison, New Jersey, NJ 08820-3097, USA), exciting the sample at 295 nm and recording the emission spectra from 310 to 410 nm. The excitation and emission slit widths were both 5 nm. Each sample was tested in duplicate. The fluorescence spectra center of mass (SCM) was calculated from the intensity data (I_λ) obtained at different wavelengths (λ) using the following equation:

$$\mathrm{SCM} = \sum \lambda^* I_\lambda / \sum I_\lambda \quad (2)$$

After correcting the fluorescence intensity data for dilution due to the addition of acrylamide, the value of the Stern–Volmer constant (K_{SV}) or dynamic quenching, was calculated from the non-linear fitting of the experimental data with the equation:

$$\frac{F_0}{F} = 1 + (K_{SV} * [A])\exp K_{ST}[A] \quad (3)$$

where F_0 and F are, respectively, the fluorescence intensities in the absence and presence of acrylamide, K_{ST} is the static quenching constant and $[A]$ is the molar concentration of acrylamide [9].

Upon completion of the fibrillogenesis, the aggregates were harvested by centrifugation, washed twice with PBS. Then, the acrylamide quenching experiments were performed again in samples containing 20 μg/ml (1.6 μM) of washed fibrils. Protein 6a-F2W was analyzed in both soluble and aggregated states.

2.7. Electron microscopy

Electron microscopy was performed at 80 kV on a Zeiss EM900 Transmission Electron Microscope (TEM), as describe previously [6].

3. Results

3.1. GndHCl- and thermal-induced equilibrium unfolding

Both GndHCl- and heat-induced unfolding curves of the Phe2 mutants showed a sigmoidal, cooperative transition that in all cases was well described by a two-state unfolding model (Fig. 1). The thermodynamic parameters calculated from the unfolding experiments are shown in Table 1. The data indicate that the most destabilizing mutation was F2P ($\Delta\Delta G_{unf}$ = 2.5 kcal mol^{-1}) and the least destabilizing substitutions were F2L ($\Delta\Delta G_{unf}$ = 1.2 kcal mol^{-1}) and F2W ($\Delta\Delta G_{unf}$ = 1.3 kcal mol^{-1}). Thus, introduction of Pro2 caused the loss of 50% of 6aJL2 folding stability, doubling the destabilizing effect caused by Leu and Trp (Table 1). In all mutants, with the exception of 6a-F2L, the ΔG_{H2O} value differs from that of $\Delta G_{25°C}$. Such differences most probably reflect inaccuracies in estimating the ΔC_p, with the subsequent miscalculation of the $\Delta G_{25°C}$.

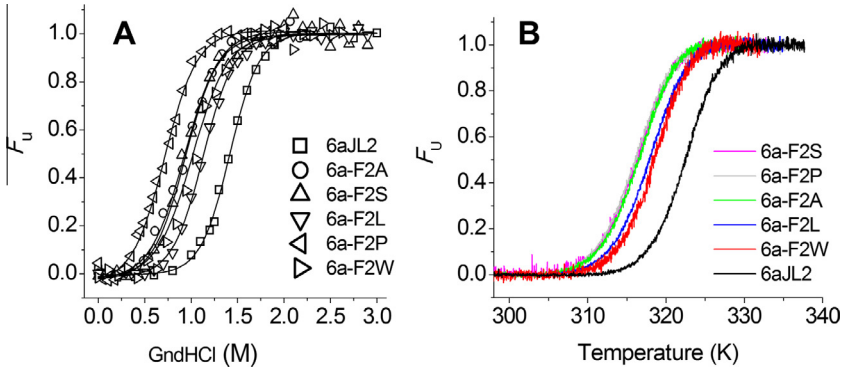

Fig. 1. Reversible unfolding experiments. (A) GndHCl and (B) heat-induced equilibrium unfolding of the wild-type protein 6aJL2 and its mutants. Data represent the variation of the fraction unfolded (F_U) as a function of the denaturant concentration (A) an temperature (B). In (A) the solid line is the non-linear fit to a two state model.

Table 1
Thermodynamics and aggregation. Parameters describing the thermodynamic stability of 6aJL2 protein and its mutants in the Phe2, as determined by equilibrium GndHCl and head induced unfolding, and the kinetic of *in vitro* fibrillogenesis without seeding.

Protein	Thermal denaturation			GndCl denaturation			$\Delta\Delta G^c$ (kcal/mol)	*In vitro* fibrilogenesis
	$\Delta G_{25\ °C}$[a] (kcal/mol)	T_m[b] (°C)	ΔH_m[b] (kcal/mol)	ΔG_{H2O} (kcal/mol)	$-m$ (kcal/mol M^{-1})	C_m (M)		t_{lag} (min)[d]
6aJL2	5.2	49.9	86.2	5.1 ± 0.5	3.6	1.41	–	900
6a-F2S	3.5	43.8	73.6	2.9 ± 0.5	3.3	0.87	1.9	56
6a-F2A	N.R.	44.3	N.R.	2.2 ± 0.3	2.5	0.87	1.9	119
6a-F2L	3.9	45.7	76.1	3.7 ± 0.2	3.4	1.09	1.2	244
6a-F2P	3.5	43.6	73.7	2.1 ± 0.3	2.9	0.71	2.5	131
6a-F2W	4.3	46.0	81.3	3.6 ± 0.5	3.4	1.04	1.3	N.D.

N.R. means non reversible.
N.D. means not determined.
[a] Calculated as described by Pace et al. [18].
[b] Calculated from the plot of ΔG versus T.
[c] Cumulative free energy change relative to 6aJL2: $\Delta\Delta G_{unf} = (m^{6aJL2} \times C_m^{mut}) - (m^{6aJL2} \times C_m^{6aJL2})$.
[d] Calculated by extrapolating the linear region of the hyperbolic phase back to the abscissa.

3.2. In vitro fibrillogenesis from the soluble precursor

All the Phe2 mutants aggregated with a profile consistent with a nucleation-dependent polymerization reaction (Fig. S3). The t_{lag} varied from one mutant to another (Table 1). The shortest t_{lag} was that of mutant 6a-F2S (56 min). In contrast, mutant 6a-F2L aggregated with the longest t_{lag}, (244 min). As evidenced by electron microscopy, the aggregates formed, in all cases, comprised mainly unbranched fibrils of variable length, characteristic of the amyloid-like fibrils (Fig. S4).

3.3. In vitro fibrillogenesis with seeding

Co-incubation of monomers and the respective homologous seeds resulted in a rapid increase in ThT fluorescence, without an appreciable t_{lag} (Fig. 2). Electron microscopy data showed that the gross morphology of all fibrils is similar, therefore if as a first approximation we assume that the binding sites and quantum yield of ThT in all fibrils are similar; then the highest ThT fluorescence intensity at the plateau in 6a-F2S ($A_{ThT} = 1.8$) suggests that it produced more ThT-binding aggregates than 6aJL2. In contrast, 6a-F2P ($A_{ThT} = 0.5$) had the lowest ThT fluorescence, suggesting a lower amount of amyloid aggregates. Interestingly, the pseudo-first order rate constant (k) of 6a-F2P ($1.16 \times 10^{-4}\ s^{-1}$) was 2.3 times higher than that of 6aJL2 (Table S5), indicating that Pro enhances the polymerization reaction. Mutations at position Pro7 and His8 modulated the kinetics of fibril elongation differently. The single P7S substitution enhanced the fibril elongation capacity of 6aJL2 ($A_{ThT} = 1.6$ and $k = 1.1 \times 10^{-4}\ s^{-1}$), whereas mutations H8P and H8S decreased it (Fig. 2 and Table S5). Notably, the double mutant 6a-P7S-H8S exhibited the greatest elongation capacity ($A_{ThT} = 2.0$), having a k value near 2.5 faster ($k = 1.2 \times 10^{-4}\ s^{-1}$) than that of the wild-type.

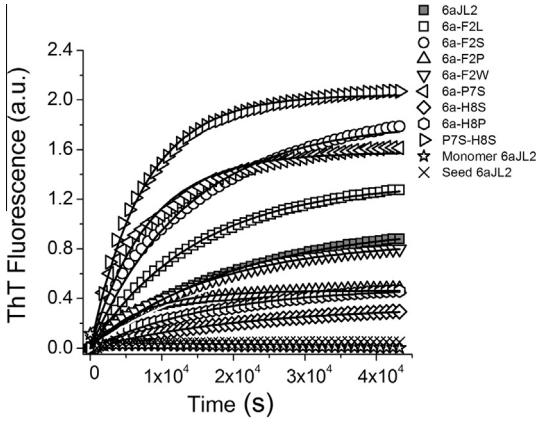

Fig. 2. *In vitro* fibrillation by seeding. Aggregation kinetics, as followed by ThT fluorescence, of 6aJL2 and its mutants by self-seeding. The data represented are the mean of quadruplicated samples. The data of the 6aJL2 soluble monomer incubated without seeding (★) and that of 6aJL2 seed incubated without monomer (×) are presented as reference. The solid line is the non-linear least-square fitting to Eq. (1).

3.4. In vitro fibrillogenesis of Trp mutants with acrylamide quenching

While 6aJL2 protein has a natural Trp at position 35, this residue contributes poorly to the intrinsic fluorescence of the molecule in

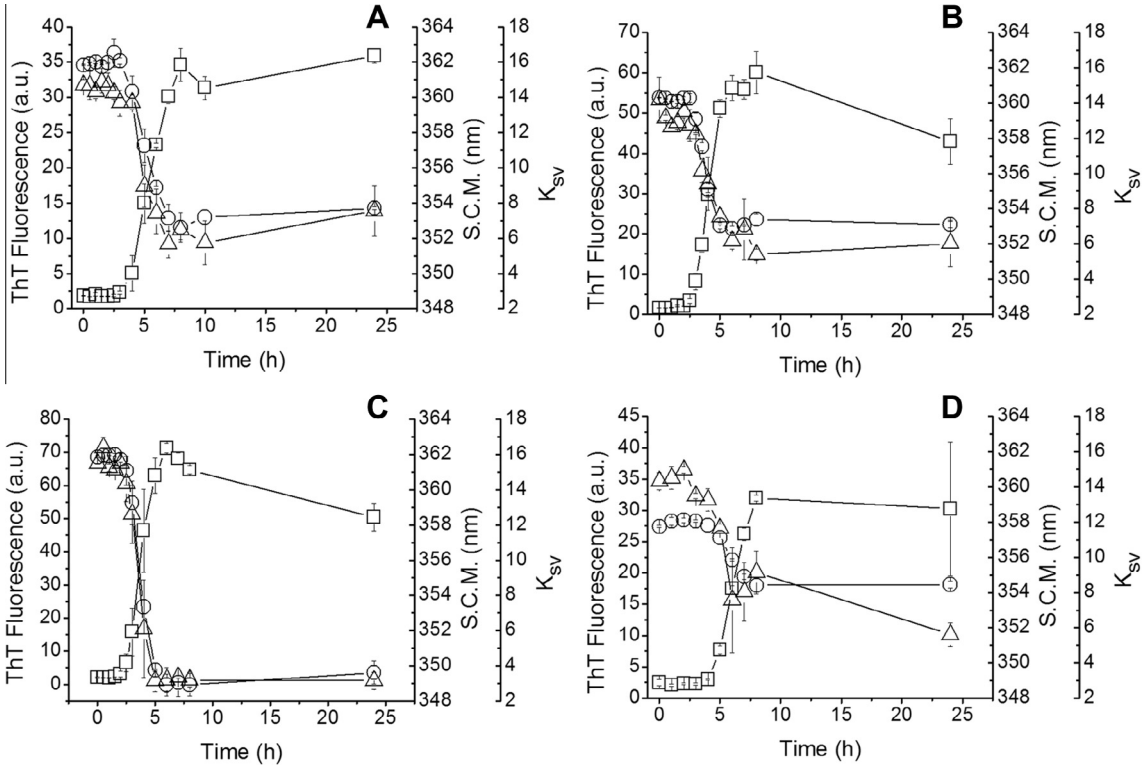

Fig. 3. Aggregation kinetics of the Trp mutants. *In vitro* fibrillogenesis of the mutant proteins (A) 6a-N1W, (B) 6a-M3W, (C) 6a-H8W, and (D) 6a-S14W. The data represented are the time-course of the ThT fluorescence (□), spectra center of mass (S.C.M.) of the intrinsic fluorescence (△) and the Stern–Volmer constant (K_{SV}) or dynamic quenching (○) determined in acrylamide quenching experiments. The error bars represent the 95% confidence intervals of duplicated samples.

native state, as it is quenched by the highly conserved intradomain disulphide bond Cys23–Cys88 [10]. The time course of the ThT fluorescence intensity of the Trp mutants at positions 1, 3, 8 and 14 displayed a sigmoidal shape, with a t_{lag} ranging from 2.4 h (6a-H8W) to 4.1 h (6a-S14W). Both, the SCM of intrinsic fluorescence and the Stern–Volmer quenching constant (K_{SV}) varied simultaneously, but in opposite direction, with respect to the ThT fluorescence intensity (Fig. 3). At the end of the experiment both variables reached similar values in mutants 6a-N1W (SCM = 353.7 nm and K_{SV} = 7.6), -M3W (SCM = 353.1 nm and K_{SV} = 6.0) and -S14W (SCM = 354.5 nm and K_{SV} = 5.6), but significantly lower in mutant 6a-H8W (SCM = 349.6 nm and K_{SV} = 3.2). In general, the fibrils collected at the end of the experiments had lower K_{SV} value than the end-point samples (Table S6).

4. Discussion

4.1. Thermodynamic stability and aggregation propensity of the Phe2 mutants

One implicit goal of this study was to evaluate the structural importance of Phe2 in λ6 light chains, as this residue is characteristic of that immunoglobulin family [3]. In the crystallographic structure of 6aJL2 protein [4] Phe2 is buried in a pocket formed by Leu4, Arg25, Ser27, Tyr91, Asp92, and Val97 (Fig. S1B). In this molecular environment, Phe2 establishes a cation-π interaction with Arg25. This type of interaction is relatively common in proteins and contributes to folding stability [11]. Thus, the thermodynamic instability associated to mutations of Phe2 can be explained, at least partially, by the disruption of this type of non-covalent bond with Arg25. However, the structural characteristics of the residue at position 2 also seem to play an important role in the domain stability, given the differences seen in each of the Phe2 mutants. We propose that such differences also reflect the ease with which the substituted residue can reside inside the apolar pocket normally occupied by the phenyl moiety of Phe2 (Fig. S1B–D). Thus, Ser and Pro were highly destabilizing substitutions at position 2 due to the small polar side chain, and structural restrictions, respectively. The side chain of Ala, despite being apolar, is too small to fill the pocket. Leu and Trp were the least destabilizing because their apolar and larger side chains likely provided the most efficient "fit" within the pocket. This hypothesis is supported by the acrylamide-quenching studies, which indicated that the Trp2 indole moiety is buried in the soluble state (Fig. S2D). Nevertheless, none of the two residues seems to optimally fill the pocket, as Leu appears to be a bit small and Trp too large (Table 1, Fig. S1C and D). Thus, our data support the fact that Phe2 contributes importantly to the thermodynamic stability of the λ6 V_L domain by its ability to fill optimally the pocket where it establish the cation-π interaction with Arg25. In a previous report it was shown that mutation R25G, which also disrupts the Arg25–Phe2 cation-π interaction, destabilizes 6aJL2 by 1.7 kcal/mol [2], an impact in folding stability similar to that of mutations F2S and F2A (in both cases $\Delta\Delta G_{unf}$ = 1.9 kcal/mol). Due to the change in side chain volume associated to R25G mutation, it is very probably that a packing defect is part of the destabilizing mechanism. It has been shown that mutations causing packing defects are generally associated with decreased stability, but the magnitude of the destabilizing effect is context-dependent [12].

Phe2 mutations accelerated, in a residue-dependent manner, the kinetic of fibrillogenesis of 6aJL2 protein, by shortening the t_{lag} of the aggregation reaction. In accord with previous reports [2,6,7,10,13], we observed a positive correlation between protein stability and the t_{lag} (Fig. S7). The correlation here appears to be non-linear, as proteins with the C_m equal or lower to 1.0 M GndHCl aggregated with similar t_{lag}, but as the C_m get larger, the t_{lag}

increased gradually. In contrast, there is not a clear correlation between the thermodynamic stability and the parameters (A_{ThT} and k) describing the kinetics of fibril elongation by homologous seeding (Fig. S7). This observation agrees with a previous report [6] and suggest differences regarding the energetic and the structural factors driving the nucleation and elongation phases of the light chain fibrillogenesis. While the first is primarily determined by the accumulation of misfolded species [13], the second appears to be influenced by specific structural characteristics of the precursor. In this regard, Masahiro Abe et al. [14] showed that sugars can retard the fibrillogenesis of the λ6 rV_L protein 3Hmut Wil by increasing its folding stability, but do not affect in the same way the elongation of the amyloid fibrils.

4.2. Role of the N-terminal strand in the mechanism of V_L fibril assembling

All the mutations tested in this study targeted the N-terminal strand. Thus, the different ability for assembling into fibrils displayed by the mutant proteins reflects to some degree the contribution of this protein segment to the mechanism of aggregation. As a trend, substitutions that introduce a Pro residue, e.g., F2P and H8P, decreased the amount of fibrils formed at equilibrium. In contrast, substituting Pro7 to Ser significantly increased fibrillar content (Fig. 2). Thus, introducing Pro in the N-terminal strand hindered 6aJL2 fibril elongation, an effect also observed in other amyloid precursors [15]. In contrast, no correlation was observed between Pro mutation and the k value, as 6a-F2P had a k value 2.5 times higher than the wild-type, but similar to 6a-P7S, in which Pro7 was substituted to Ser (Table S5). Our data suggest that both the kinetics and the energy of 6aJL2 fibril elongation can be modulated by multiple, varied mutations at the N-terminal strand. These findings indicate that the N-terminal strand may be involved not only in stabilizing the global immunoglobulin domain, but also may participate in the network of contacts required for fibrillogenesis.

To get insight about the location of the N-terminal strand in the fibrillar state, we generated single Trp mutants at four different positions along the N-terminal strand (Fig. S2A). Then, we studied the hydration state of these residues during the assembly process, by taking advantage of the dependence of the Trp fluorescence upon environment [16] (Fig. S2B). We found that each of the N-terminal Trp residues enters a more hydrophobic environs as the V_L assembles into fibrils (Fig. 3). The most dramatic change in solvent exposure, as determined by acrylamide quenching, was that of 6a-H8W, while it was similar for the other Trp mutants (Fig. S2C, Table S6). The scarcity of data regarding the AL fibril structure make it difficult to interpret these findings. However, we postulate that either the N-terminal strand adopts a novel configuration, such as the previously proposed type 6 β turn [17], or perhaps becomes incorporated into the core or solvent inaccessible region of the amyloid-like fibril.

In summary, here we have shown that mutations at the N-terminal strand of 6aJL2 protein modulate both the folding thermodynamics and the fibrillogenesis of the molecule. Furthermore, we have data that suggest that the N-terminal strand is less solvent accessible in the fibrillar state, possibly being accommodated in the proximity of the fibril β-core. Based on these findings, we propose that the N-terminal strand is a potential target for developing an inhibitor-based therapeutic approach in AL amyloidosis.

Acknowledgments

This work was supported in part by Grants from the Consejo Nacional de Ciencia y Tecnología (CONACYT) (No. 169659 to L. del Pozo-Yauner and No. 102182 to D.A. Fernández Velasco) and intramural financing (INMEGEN research project 084) to L. del Pozo-Yauner.

Appendix A. Supplementary data

Supplementary data associated with this article can be found, in the online version, at http://dx.doi.org/10.1016/j.bbrc.2013.11.123.

References

[1] R. Khurana, J.R. Gillespie, A. Talapatra, L.J. Minert, C. Ionescu-Zanetti, I. Millett, A.L. Fink, Partially folded intermediates as critical precursors of light chain amyloid fibrils and amorphous aggregates, Biochemistry 40 (2001) 3525–3535.
[2] L. del Pozo Yauner, E. Ortiz, R. Sanchez, R. Sanchez-Lopez, L. Guereca, C.L. Murphy, A. Allen, J.S. Wall, D.A. Fernandez-Velasco, A. Solomon, B. Becerril, Influence of the germline sequence on the thermodynamic stability and fibrillogenicity of human lambda 6 light chains, Proteins 72 (2008) 684–692.
[3] P.R. Pokkuluri, A. Solomon, D.T. Weiss, F.J. Stevens, M. Schiffer, Tertiary structure of human lambda 6 light chains amyloid, Int. J. Exp. Clin. Invest. Official J. the Int. Soc. Amyloidosis 6 (1999) 165–171.
[4] A. Hernandez-Santoyo, L. del Pozo Yauner, D. Fuentes-Silva, E. Ortiz, E. Rudino-Pinera, R. Sanchez-Lopez, E. Horjales, B. Becerril, A. Rodriguez-Romero, A single mutation at the sheet switch region results in conformational changes favoring lambda6 light-chain fibrillogenesis, J. Mol. Biol. 396 (2010) 280–292.
[5] J.S. Richardson, D.C. Richardson, Natural beta-sheet proteins use negative design to avoid edge-to-edge aggregation, Proc. Natl. Acad. Sci. USA 99 (2002) 2754–2759.
[6] M. Gonzalez-Andrade, B. Becerril-Lujan, R. Sanchez-Lopez, H. Cecena-Alvarez, J.I. Perez-Carreon, E. Ortiz-Suri, D.A. Fernandez-Velasco, L. Del Pozo-Yauner, Mutational and genetic determinants of lambda6 light chain amyloidogenesis, FEBS J. 280 (2013) 6173–6183.
[7] J. Wall, M. Schell, C. Murphy, R. Hrncic, F.J. Stevens, A. Solomon, Thermodynamic instability of human lambda 6 light chains: correlation with fibrillogenicity, Biochemistry 38 (1999) 14101–14108.
[8] N. Takahashi, K. Hasegawa, I. Yamaguchi, H. Okada, T. Ueda, F. Gejyo, H. Naiki, Establishment of a first-order kinetic model of light chain-associated amyloid fibril extension *in vitro*, Biochim. Biophys. Acta 1601 (2002) 110–120.
[9] P.O. Souillac, V.N. Uversky, A.L. Fink, Structural transformations of oligomeric intermediates in the fibrillation of the immunoglobulin light chain LEN, Biochemistry 42 (2003) 8094–8104.
[10] M.R. Hurle, L.R. Helms, L. Li, W. Chan, R. Wetzel, A role for destabilizing amino acid replacements in light-chain amyloidosis, Proc. Natl. Acad. Sci. USA 91 (1994) 5446–5450.
[11] R.S. Prajapati, M. Sirajuddin, V. Durani, S. Sreeramulu, R. Varadarajan, Contribution of cation-π interactions to protein stability, Biochemistry 45 (2006) 15000–15010.
[12] A.E. Eriksson, W.A. Baase, X.J. Zhang, D.W. Heinz, M. Blaber, E.P. Baldwin, B.W. Matthews, Response of a protein structure to cavity-creating mutations and its relation to the hydrophobic effect, Science 255 (1992) 178–183.
[13] Y. Kim, J.S. Wall, J. Meyer, C. Murphy, T.W. Randolph, M.C. Manning, A. Solomon, J.F. Carpenter, Thermodynamic modulation of light chain amyloid fibril formation, J. Biol. Chem. 275 (2000) 1570–1574.
[14] M. Abe, Y. Abe, T. Ohkuri, T. Mishima, A. Monji, S. Kanba, T. Ueda, Mechanism for retardation of amyloid fibril formation by sugars in Vlambda6 protein, Protein Sci.: Publ. Protein Soc. 22 (2013) 467–474.
[15] A.D. Williams, E. Portelius, I. Kheterpal, J.T. Guo, K.D. Cook, Y. Xu, R. Wetzel, Mapping abeta amyloid fibril secondary structure using scanning proline mutagenesis, J. Mol. Biol. 335 (2004) 833–842.
[16] J.T. Vivian, P.R. Callis, Mechanisms of tryptophan fluorescence shifts in proteins, Biophys. J . 80 (2001) 2093–2109.
[17] B. O'Nuallain, A. Allen, S.J. Kennel, D.T. Weiss, A. Solomon, J.S. Wall, Localization of a conformational epitope common to non-native and fibrillar immunoglobulin light chains, Biochemistry 46 (2007) 1240–1247.
[18] C.N. Pace, Determination and analysis of urea and guanidine hydrochloride denaturation curves, Methods Enzymol. 131 (1986) 266–280.